A Simulation Analysis of Grid-Connected DSTATCOM with PWM Voltage Control and Hysteresis Current Control for Power Quality Improvement

Research paper

Minesh K. Joshi*[ID], R. R. Patel*[ID]

Department of Electrical Engineering, The Charutar Vidya Mandal (CVM) University, Anand, Gujarat, India

Abstract: The DTSTACOM is a power quality compensator that can be used in the distribution grid to compensate the demand of reactive power, which can be produced by different linear and non-linear loads. In this process, the control method of DSTATCOM is one of the key factors influencing the performance of DSTATCOM. This study aims to analyse the effect of two modulation schemes, Pulse Width Modulation (PWM) and Hysteresis Current Control (HCC), under several conditions. The proposed modelling approach and Synchronous Reference Frame (SRF) theory are used to verify reactive power compensation and total harmonic distortion (THD). Further, PWM and Hysteresis Current Control (HCC) with proportional-integral (PI) controller simulated in MATLAB for different cases, and percentage THD was calculated to prove the effectiveness of the proposed method for the control of reactive power and THD with grid-connected DSTATCOM. The results presented here justify that the HCC controller can be better than the PWM method to generate the PWM pulses for reduction of harmonics under various conditions of DTSTACOM to compensate the reactive power. Additionally, the simulation was performed to check the efficacy of the projected method to reduce THD by varying the current control band of HCC.

Keywords: DSTATCOM • reactive power • proportional integral • hysteresis current controller • total harmonic distortion

1. Introduction

Power quality issues are more prevalent in today's power systems. Many factors, including rising demand for electric energy, deregulation and economic and environmental constraints on expanding power networks, have forced power systems to operate at or near their stability limits. Flexible AC Transmission Devices (FACTS) have shown superiority in the last few decades in managing the demand for lower power losses and quicker response to system performance under transient conditions with higher stability (Pasrba, 2004). FACTS has become the choice to manage voltage control, and reactive power under steady state and dynamic conditions in the power system, based on successful research in power electronics switching devices (Bollen, 1999; Hingorani and Gyugyl 1999). The DSTATCOM is a piece of shunt-connected power equipment used to inject current at the point of common coupling (PCC) in the distribution power system (Edris, 2000). A combination of different loads is connected to the PCC, which draws harmonics and reactive current from the generating sources in the grid and reduces the power quality (Kamel and Fenghua, 2020; Pal et al., 2011). A comparative study has been discussed with different operating modes of the STATCOM in weak AC networks and proven satisfactory results (Khatir et al., 2012). A robust design for current controller STATCOM and healthy voltage controller-based STATCOM was demonstrated using a simple loop method (Singh et al., 2015). The genetic algorithm and optimisation technique proposed to

analyse overshoot, settling time and different operating modes of the STATCOM (Safari et al., 2013). Furthermore, proportional-integral (PI) controllers, which provide stabilised controls, have always been an important component of control systems (Li et al., 2013; Rahim and Kandlawala, 2004). The different techniques (Chebabhi, 2016) were developed to improve the overall efficiency of the distribution grid with stable voltage. One of the modulation techniques used in DSTATCOM, an adaptive PID controller-based technique, produces better results, particularly in noisy systems (Chothani et al., 2021). Non-linear load compensation was performed using the PI controller's inner and outer loops to identify power quality issues and harmonics. Simulation for optimum symmetric criteria has been revealed by the authors (Tripathi, 2018). The topology of SVC with hybrid DSTATCOM was simulated with HCC under different unbalanced loading conditions to minimise the harmonic distortions (Mangaraj and Sabat, 2023). Constant-frequency HCC for three-phase VSI has been discussed in digital signal controllers and proved experimentally to reduce harmonic distortion as per the IEEE 519 standard (Kalyanraj and Lenin Prakash, 2014). Several methods, such as hysteresis control, predictive-based control, self-tuning filter theory and cross-correlation theory, have been proposed for STATCOM control to improve the performance of compensation in reactive power with STATCOM (Amoozegar, 2016). The method based on the current error space vector (CESP) for the hysteresis current controller is applied, and it is figured out that the controller provided a fast dynamic response (Raju et al., 2020). The hysteresis band (HB) control method is applied to STATCOM to maintain the voltage profile in the network. It has been proven that the STATCOM voltage profile effectively improved in a transmission line (Ngasop and David, 2020). The study was carried out for the analysis and performance estimation of a STATCOM with fast dynamic reaction for large abrupt deviations in load and grid DC bus voltage with a PI controller (Marei et al., 2004). To reduce switching frequency and current error, an algorithm is proposed to apply a zero-voltage vector in a synchronous rotating frame, and it has been proved that modified current controllers work more effectively than conventional ones in various cases (Eun and Sang, 2004). A HB current controller is used for a five-level NPC-type G converter. It has been proven through the simulation that by increasing the HB, the switching frequency reduces and consequently switching losses, hence the harmonic distortion (Daniel and Ramin, 2018). A novel current control strategy using fuzzy logic controllers for hysteresis current control was proposed and analysis was carried out and concluded that APF performance under a typical serious non-linear load condition worked smoothly (Liu et al., 2012). A detailed investigation was carried out by comparing two modulation schemes, Pulse Width Modulation (PWM) and HCC. The performance analysis was carried out during steady-state and transient conditions in PSCAD simulation (Deng, 2007). Additionally, in this study, further research is focused on unbalanced and non-linear load conditions and total harmonic distortion (THD). A detailed comparative analysis was carried out to prove the control algorithm.

In this paper, a systematic procedure for a three-phase VSC-based DSTATCOM, embracing the sizing of components and tuning of inner and outer loop PI controllers, respectively. The problem definition and proposed methodology are discussed in Section 2. The sizing of various system components and tuning of the PI controller's inner and outer loops are elaborated in Section 3. Section 4 presents the Hysteresis Current Controller (HCC) methodology, and Section 5 discusses simulation verification of the proposed DSTATCOM control method. In Section 6, some conclusions are drawn and it is proved that the HCC controller is superior to the PWM method in reducing THD. The effectiveness of the proposed method simulated in MATLAB with various cases was compared and demonstrated by the performance of DSTATCOM to compensate for the reactive power in the grid**.**

2. Proposed Methodology for DSTATCOM Control

In the power system network, reactive power compensation is required as the load demand may vary to preserve the power quality. So a reactor and switchable capacitor are required in the system to absorb and feed reactive power into the system. The authors have considered different load levels over here. To release the stress of the network, DSTATCOM compensates the reactive power demand as and when it is required.

As shown in figure 1, the three-phase source, VSC-based DSTATCOM and Loads are connected at the PCC. The inner and outer loops are current and voltage control loops respectively controlled by PI controller. The outer voltage PI controller generates direct axis source current reference value as follows:

$$I_d^* = K_{pr} \frac{(1 + Tos)*(Vdc^* - Vdc)}{Tos} \qquad (1)$$
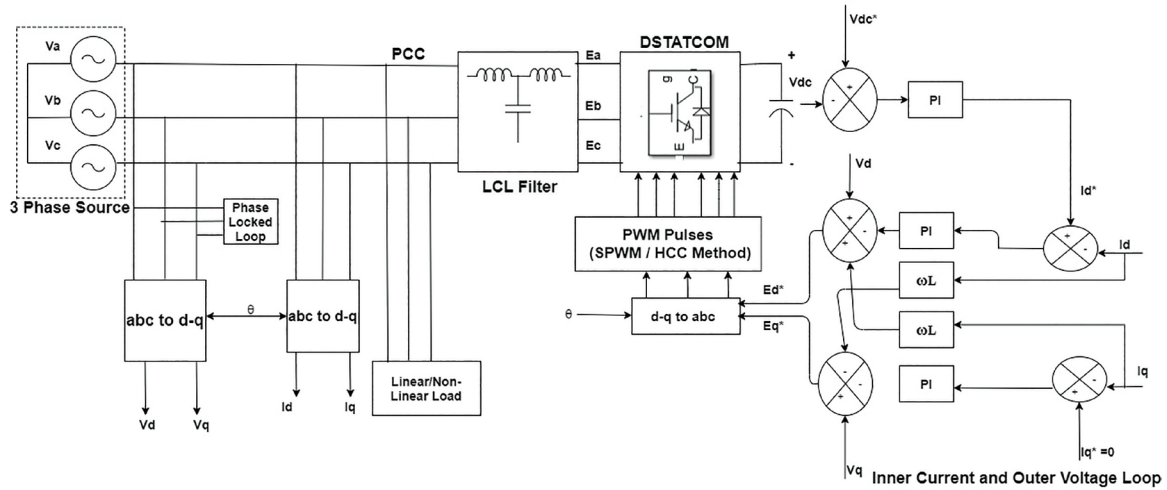
Figure 1. Schematic of the proposed DSTATCOM control Method in Distribution Network. PCC, point of common coupling.

In contrast to direct control methodology, the proposed control method is an indirect current control strategy, where the control is based on source current regulation with the quadrature current component forced to be zero. Thus, only the active current is drawn from the source, and the reactive power of the load is compensated by DSTATCOM. In comparison to the direct control method, the proposed method has the advantage of requiring fewer current sensors. If V is the peak value of the voltage at PCC, then the three-phase AC voltage as follows:

$$V_a = V\cos(\omega t) \tag{2}$$

$$V_b = V\cos(\omega t - (2\pi/3)) \tag{3}$$

$$V_c = V\cos(\omega t + (2\pi/3)) \tag{4}$$

Thus, the voltage relationship between the PCC and DSTATCOM is expressed as

$$V_a = RI_a + L(dI_a / dt) + E_r \tag{5}$$

$$V_b = RI_b + L(dI_b / dt) + E_y \tag{6}$$

$$V_c = RI_c + L(dI_c / dt) + E_b \tag{7}$$

Transform the above equation into d–q reference frame, and then it can be expressed as

$$L(dI_d / dt) = -RI_d + \omega LI_q + V_d - E_d \tag{8}$$

$$L(dIq / dt) = -\omega LI_d - RI_q + V_q - E_q \tag{9}$$

The voltage equations of each axis are cross-coupled; to decouple them, the inner current control loop and reference current of the DSTATCOM voltage can be expressed as follows:

$$E_d{}^* = V_d - \omega LI_q - \Delta V_d \tag{10}$$

$$E_q{}^* = V_q - \omega LI_d - \Delta V_q \tag{11}$$

where $E_d{}^*$ and $E_q{}^*$ are the reference values of the direct axis and quadrature axis of the DSTATCOM voltages.

To generate PWM signals, the reference DSTATCOM voltages are transformed back into a-b–c reference frame with the help of a phase-locked loop (PLL). A PLL system quickly and accurately finds out the phase angle and frequency of grid voltages. The following control diagram for PLL is used in the proposed methodology as shown in figure 2(a).

The necessity of a PLL is to get active (P) and reactive (Q) components. Through a closed-loop control, a reactive component is calculated. Here, abc to α–β and to d–q transformations are used to give input to the PI controller, and hence, P and Q are calculated through closed-loop controllers. Here, V_{qref} is taken as zero because direct axis voltage V_d is aligned with grid voltage V_{grid}.

$$\Delta V_d = K_{pr} \frac{(1 + Tis)*(Id^* - Id)}{Tis} \tag{12}$$

$$\Delta V_q = K_{pr} \frac{(1 + Tis)*(Iq^* - Iq)}{Tis} \tag{13}$$

where $T_i = K_{pr}/K_{ii}$ and K_{pr} = Proportional gain and K_{ii} = Integral gain.

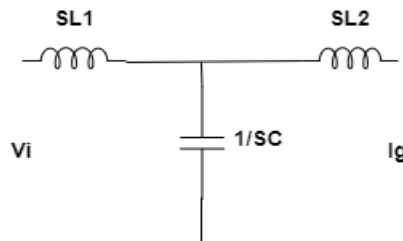# 3. Component Sizing and Tuning of Inner Current and Outer DC Voltage PI Controller

A. Component Sizing (Tripathi, 2018):

From the figure 2(b) the transfer function for the LCL filter circuit can be calculated as

$$\frac{Ig}{Vi} = \frac{1}{sL(1 + s^2CLp)}. \tag{14}$$
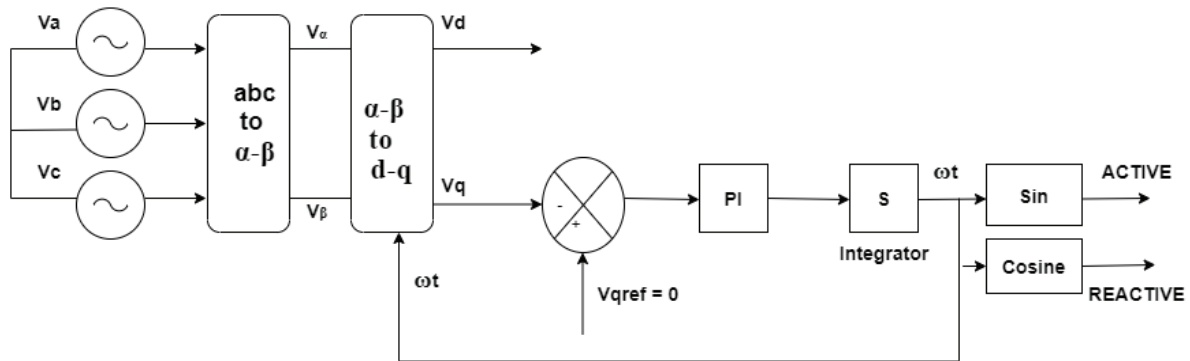
(a)

(b)

Figure 2. (a) PLL. PI, proportional integral; PLL, phase locked loop. (b) LCL Filter Sizing and Calculation (Deng, 2007).

Depending on the requirement of reactive power as a thumb rule, the reactive power absorbed by the capacitor is 5% of the rated power which is chosen. I_g is the grid current and V_i is the inverter side voltage, $L_p = L_1L_2/L_1 + L_2.$

$$Q = \frac{V^2}{(1/2*pi*f*C)} = 5\% \text{ of } S. \tag{15}$$

The value of Capacitance can be formulated as

$$C = \frac{0.05*S}{V^2*2*pi*f} \tag{16}$$

where S is the rated power = 1,000 kVA, V = V_{grid} = 230 V per phase, f = 50 Hz taken for the calculation, and hence, the calculated value of the capacitance of a capacitor is selected as 100.28 μF. However, 100 μF is used in the simulation.

The value of inductance can be calculated from Eq. 14 by replacing term CL_p in terms of resonance frequency (ω_{res}) and solving in terms of L

$$L = \frac{1}{\omega_{sw}*\left(\frac{I_{g(sw)}}{V_{i(sw)}}*\left(1-\left(\frac{\omega_{sw}^2}{\omega_{res}^2}\right)\right)\right)}. \tag{17}$$

The switching frequency is selected as 10 kHz and resonance frequency is taken as 1 kHz. According to the thumb rule, $I_{g\,(sw)}$ is taken 0.3% of the grid current (I_g) and $V_{i\,(sw)}$ is taken 0.9 times the grid voltage (V_g). The voltage drops across both inductors always limited to 20% of grid voltage is chosen. So, considering $L_1 = L_2$, the value of Inductance can be given as

$$L_1 = L_2 = \left(\frac{L_{max}}{2}\right) = \frac{0.2*Vgrid}{2*pi*50*I}. \tag{18}$$

Here, the Inductance of Inductor is selected as 500 μF.

B. Tuning of Inner Current PI Controllers

In the schematic of figure 1, the inner current control loop is demonstrated in the synchronously rotating d–q axis source currents. The control configuration is used by a conventional PI controller to maintain voltage amplitude at the PCC by controlling the amplitude or changing DSTATCOM output voltage. The generated error signal is processed by inner PI current controllers. Thus d–q axis currents follow their reference values only. The open loop transfer function can be expressed as

$$G_{OL\_i}(S) = \frac{I_q}{I_q^*} = \frac{I_d}{I_d^*} = \frac{\left(K_{pr}*S + K_{ii}\right)}{S} * \frac{1}{\left(L_{sh}*S + R_{sh}\right)}. \tag{19}$$

Thus, the closed-loop transfer function can be obtained by the following equation:

$$G_{CL\_i}(S) = \frac{\left(K_{pr}*S + K_{ii}\right)}{\left(S^2 + \left(\frac{Rsh}{Lsh} + K_{pr}\right)*S + K_{ii}\right)} \tag{20}$$

The proportional and integral controller gain of current controller loop is intended through pole imposition method as discussed in Kamel and Fenghua (2020). The identification with the canonical function developed by the Ziegler–Nicholas tests and thus the coefficient of both gains K_{pr} and K_{ii} will be given as:

$$K_{pr} = 2\rho^{(-R_{sh}/L_{sh})} \tag{21}$$

$$K_{ii} = \omega^2 \tag{22}$$

C. Tuning of Outer DC Voltage PI Controllers

From figure 1, the DC bus voltage transfer function with an open loop PI controller is expressed as:

$$G_{OL\_DC}(S) = \frac{V_{dc}}{V_{dc}^*} = \frac{\left(K_{pr\_dc}*S + K_{ii\_dc}\right)}{S} * \frac{1}{(CS)} \tag{23}$$

Thus, the closed-loop transfer function is obtained by the following equation:

$$G_{CL\_DC}(S) = \frac{\dfrac{\left(K_{pr\_dc}*S + K_{ii\_dc}\right)}{C}}{S^2 + \left(K_{pr\_dc}*S/C\right) + \left(K_{ii\_dc}/C\right)} \tag{24}$$

Thus, the coefficient of both the gains are calculated in the same previous way as discussed and can be given as:

$$K_{pr\_dc} = 2\rho C \tag{25}$$

$$K_{ii\_dc} = \omega^2 C \tag{26}$$

4. Hysteresis Current Controller

The classical control technique based on PWM such as PWM, SPWM and SVM requires the precise knowledge of the load model which is the main factor for the synthesis of PI controllers to generate voltage pulses for VSC. In case the load model is not defined, then PWM control techniques have poor performance against non-linear Hysteresis Current control (HCC) (Ngasop and David, 2020). The main advantage of hysteresis current controller is that it can be applied even when the load model is not specified. The hysteresis current controller is one of the simple techniques widely used for grid-connected inverter. A fixed HB width for upper and lower range is used to control the error of current within its range. The error between both reference and measure current is controlled in a region containing upper and lower limits of HB. The principle of the method is described in figure 3(a) and figure 3(b). If the measured current is greater than the reference current of the upper band (UB) then the top switches are on. If the measured current is less than the lower band (LB) then the bottom switches are on.

The HB width can be determined as:

$$HB = \frac{\left(V_{dc}^2 - V_{grid}^2\right)}{4V_{dc}L_{fs}} \tag{27}$$

(a)

(b)
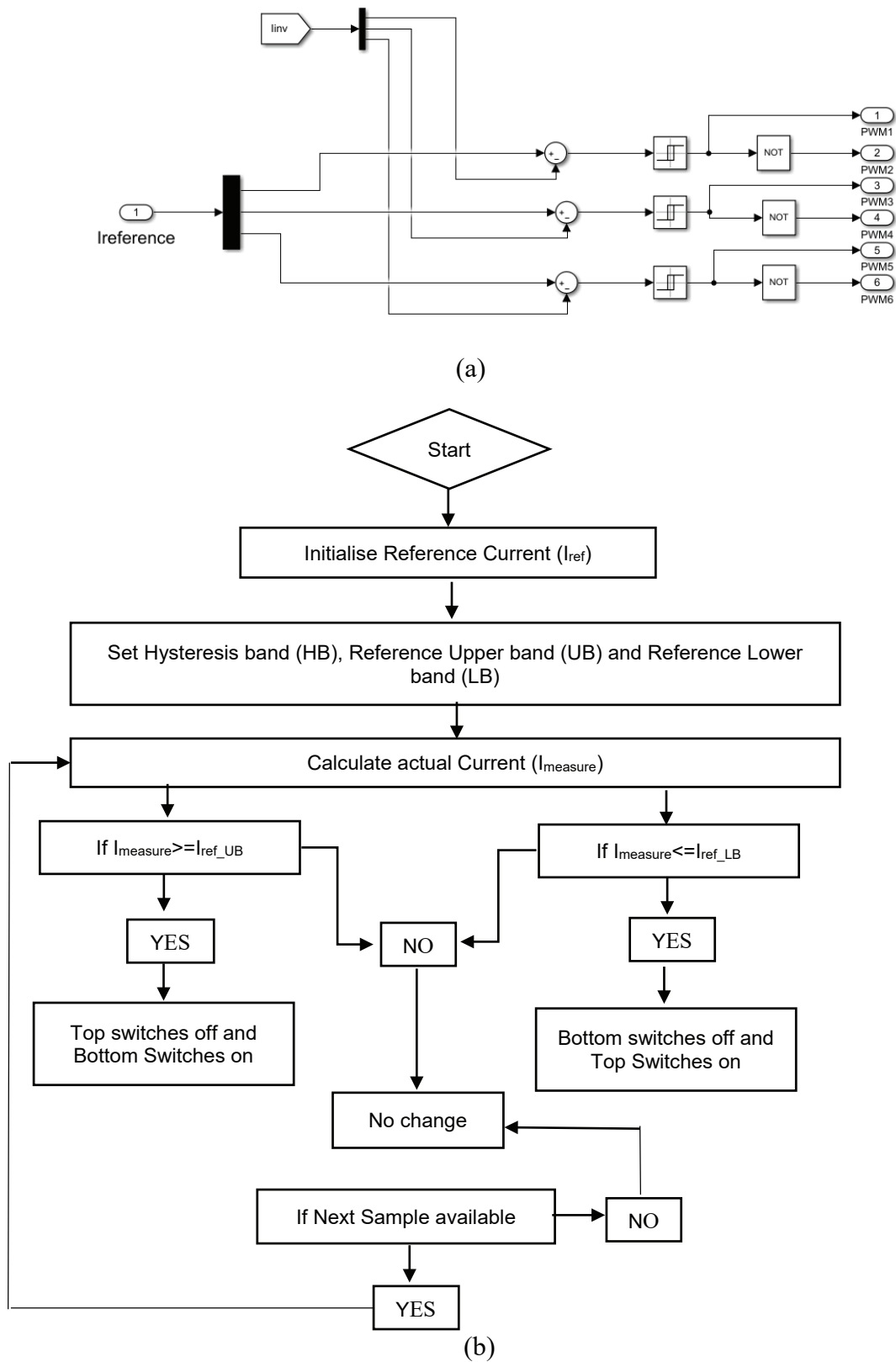
Figure 3. (a) Block diagram of Hysteresis Current Controller. (b) Flow chart of Constant frequency Hysteresis Current Controller. HB, hysteresis band; LB, lower band; PWM, Pulse Width Modulation; UB, Upper band.

5. Simulation Verification of the Proposed DSTATCOM Control Method

In this simulation part under the MathWorks MATLAB-R2019a /Simulink environment, DSTATCOM control is discussed with the power distribution grid through inner and outer loop control of PI controller. The simulation parameters and cases are stated in Table 1 (Tripathi, 2018) and Table 2 (Daniel and Ramin, 2018).

5.1. PI with PWM

To confirm the practicability, PIs with PWM are used for DSTATCOM. The various cases are simulated and discussed with linear, non-linear load and unbalanced conditions using a programmable voltage source. However, for simplicity, the percentage THD of source current in the R phase is calculated and presented in the output waveforms.

Case 1: $P_L = 100$ kW and $Q_L = 75$ kVAR

In this case, $V_{dc} = 800$ V, $P_L = 100$ kW and $Q_L = 75$ kVAR were considered. The V_{abc} and I_{abc}) observed were sinusoidal from the figure 4(a) and figure 4(b). The inverter current and load current are sinusoidal too. The figure 5(a) and figure 5(b) shown that grid sends active power of 100 kW, while DSTATCOM meets the load's reactive power demand of 75 kVAR. The voltage V_{dc} is maintained constant at 800 V. The percentage of THD observed in figure 6 is 0.82 (Tripathi, 2018).

Case 2: Performance Under extra load P = 50 KW, Q = 7.5 kVAR with Load Breaker Closed Unexpectedly

The three-phase RL load relates to the system, and the load breaker is closed at 0.15 s. So, here, the additional load gets raised. It should be noted that the demand for reactive power was raised and satisfied by DSTATCOM even after connecting an additional load for a fraction of a seconds.

The results from figure 7 demonstrate that the load demand is completely satisfied, but a time variation of 0.15 s to 0.20 s is observed in reactive power when the load breaker is closed, and it is changed from 95 kVAR to 90 kVAR. The percentage THD is 2.79 observed in the source current in figure 8.

Table 1. Simulation parameters.

| Parameters	Value
Voltage (V_{LL}), Frequency (f)	415 V, 50 Hz
Switching frequency (f_s)	10 kHz
Inductor (L)	500 μH
DC link capacitor (C), Capacitor (C)	5,000 μF, 100 μF
DC voltage (V_{dc})	800 V
Rated power	100 kVA
Fault resistance (R_f)	10 Ω
Proportional gain constant (K_{pr}) (Inner current loop)	25 V/A
Integral gain constant (K_{ii}) (Inner current loop)	500 V/A
Proportional gain constant (K_{pr_dc}) (Outer voltage loop)	5 A/V
Integral gain constant (K_{ii_dc}) (Outer voltage loop)	100 A/V
HB (Upper and lower range)	$\pm$ 0.01 A

HB, hysteresis band.

Table 2. Simulation analysis with different loading conditions.

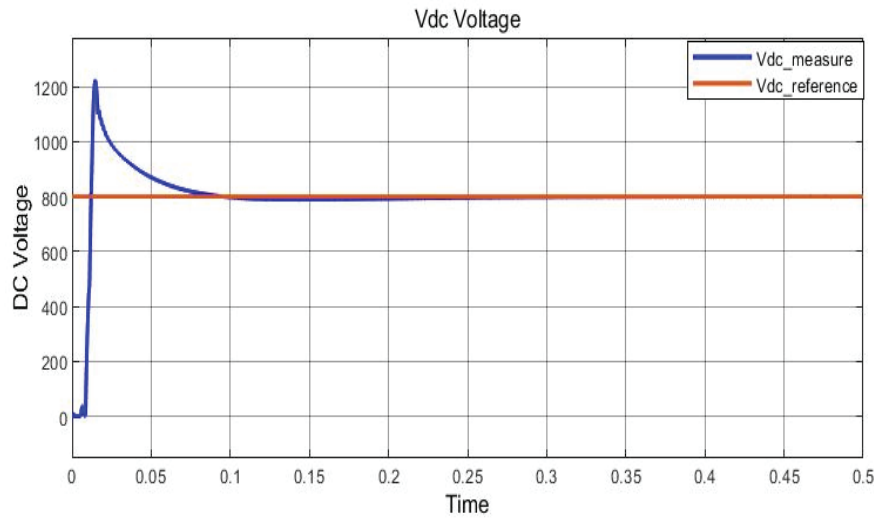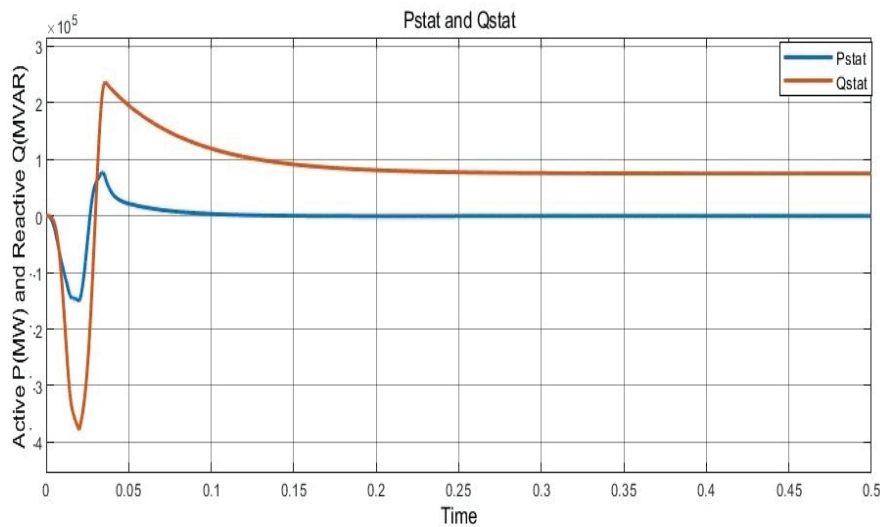| Case	Load
1	$P_L = 100$ kW, $Q_L = 75$ kVAR
2	$P_L = 100$ kW, $Q_L = 75$ kVAR, additional $P_L = 50$ kW, $Q_L = 7.5$ kVAR, Breaker closed
3	$P_L = 100$ kW, $Q_L = 75$ kVAR, additional $P_L = 50$ kW, $Q_L = 7.5$ kVAR with Non-linear load, breaker closed
4	Voltage violation at source end with $P_L = 100$ kW, $Q_L = 75$ kVAR, additional $P_L = 50$ kW, $Q_L = 7.5$ kVAR with Non-linear load
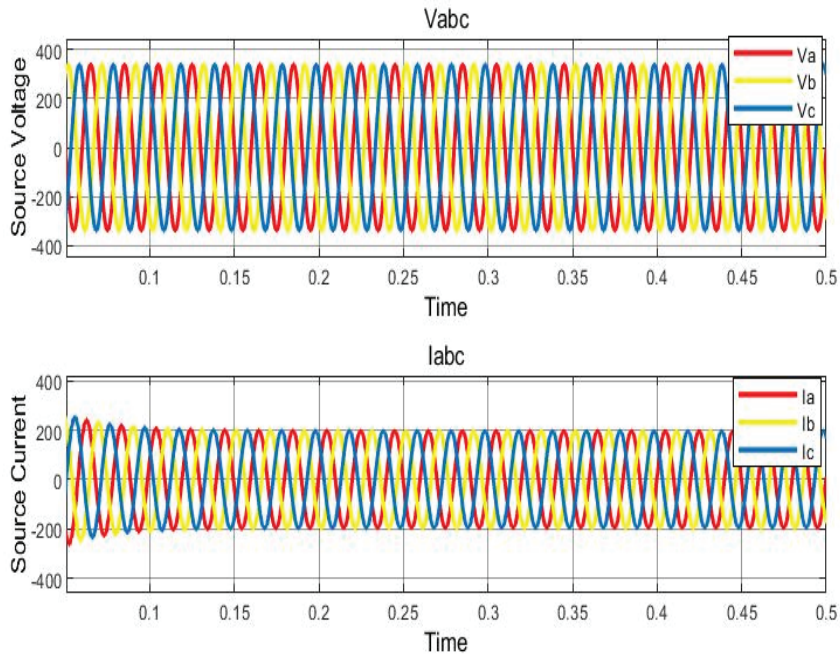
(a)
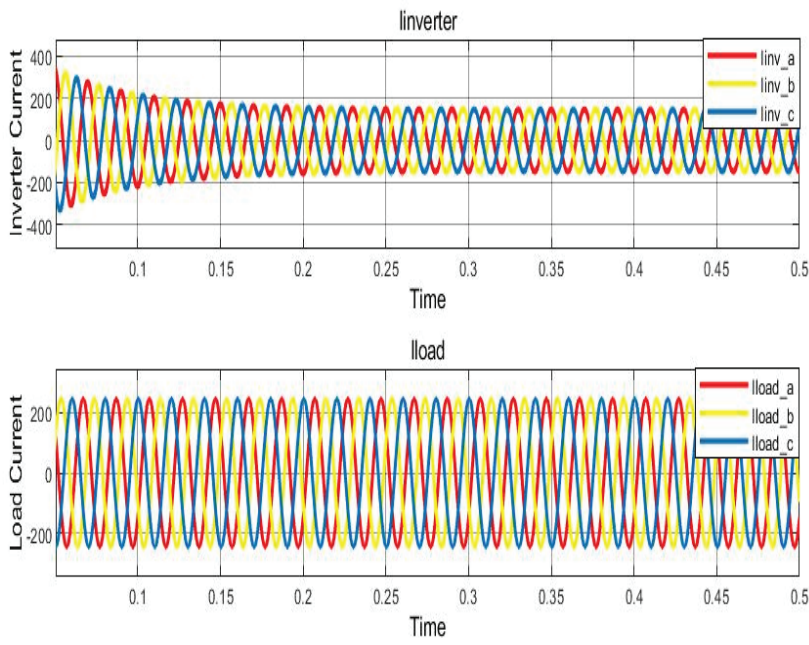
(b)

Figure 4. (a) V_{abc} and I_{abc} at Source. (b) I_{inv} and I_{load} at Inverter.

(a)

(b)

Figure 5. (a) V_{dc} measured and V_{dc} reference. (b) $P_{statcom}$ and $Q_{statcom}$.

Case 3: Non-Linear Load

Here, a non-linear load is connected in addition to the above load. The minor variation was observed in figure 9 from 0.15 s to 0.18 s. The observation shows that the non-linear load currents are effectively compensated by DSTATCOM during switching conditions. Moreover, in the presence of a non-linear load, from the figure 10 the percentage of THD is 4.13, within the marginal limit (Tripathi, 2018).

Case 4: Voltage Violation at source end and Non-Linear Load

In this case, from the figure 11 the programmable voltage source is used and violation is created at the instant of 0.2 s, 0.3 s and 0.4 s. At 0.15 s the load breaker switch is closed and non-linear load is connected with the system in addition to 150 kW and 82.5 kVAR load. The non-linear load consists of R = 20Ω, L = 0.01 × 10⁻⁹ H and C = 5 × 10⁻¹⁵ F with a diode bridge connected to the system.
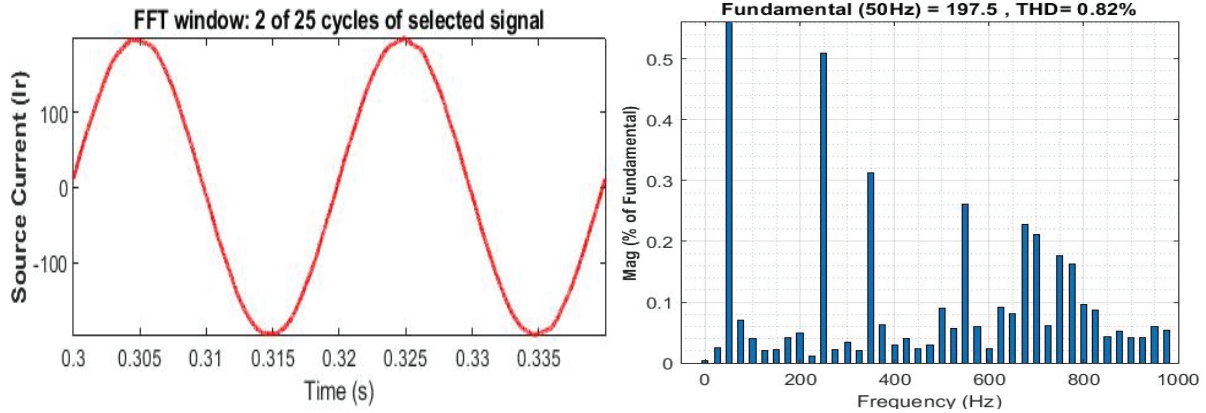
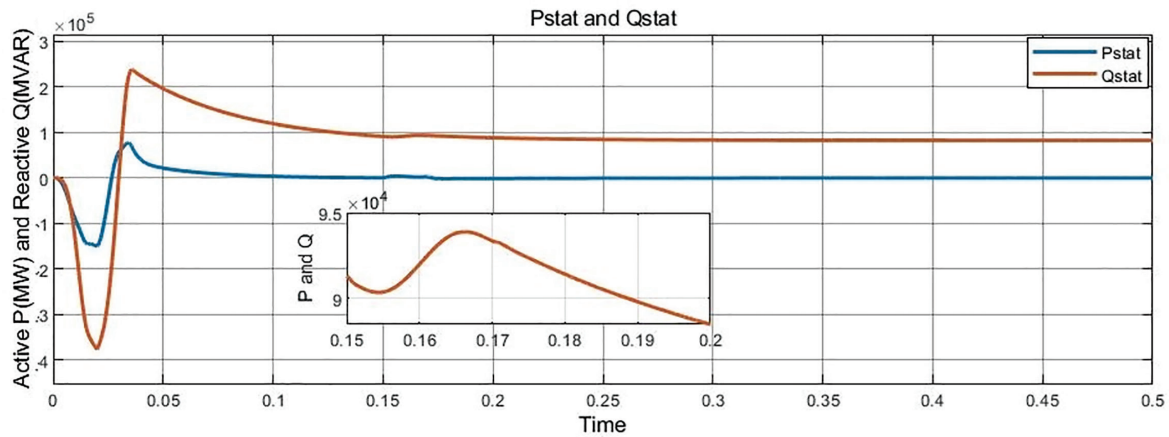**Figure 6.** Source Current (I$_r$) and Percentage of THD. THD, total harmonic distortion.

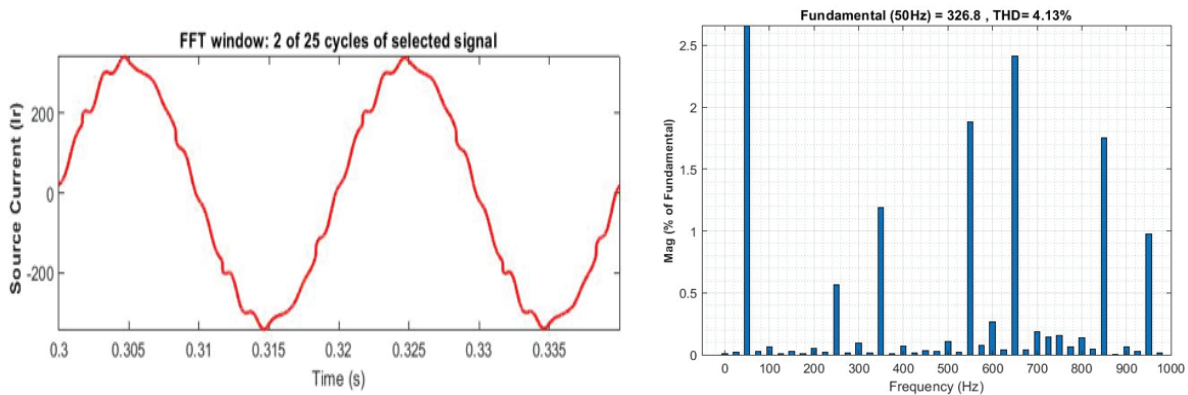**Figure 7.** P$_{statcom}$ and Q$_{statcom}$ Load Breaker Closed Unexpectedly.

Figure 8. Source Current (I$_r$) and Percentage of THD when breaker closed. THD, total harmonic distortion.

A close observation and keeping in mind that using the programmable voltage source at different instants of violation demand is completely satisfied. The satisfactory results observed to feed reactive power during the defilement with the percentage THD in the source current are 4.56 observed from the harmonic spectra of figure 12.
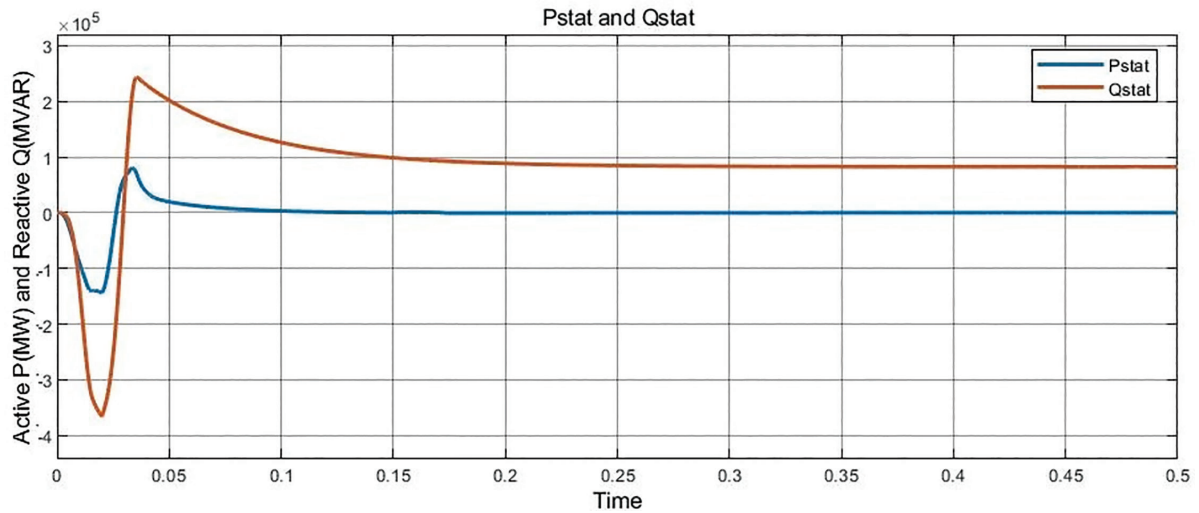
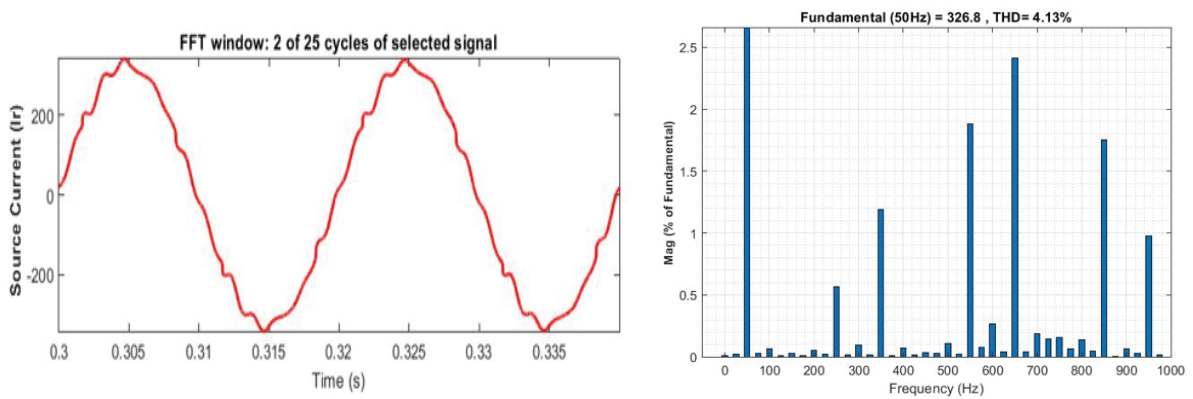**Figure 9.** $P_{statcom}$ and $Q_{statcom}$ Non-Linear Load.

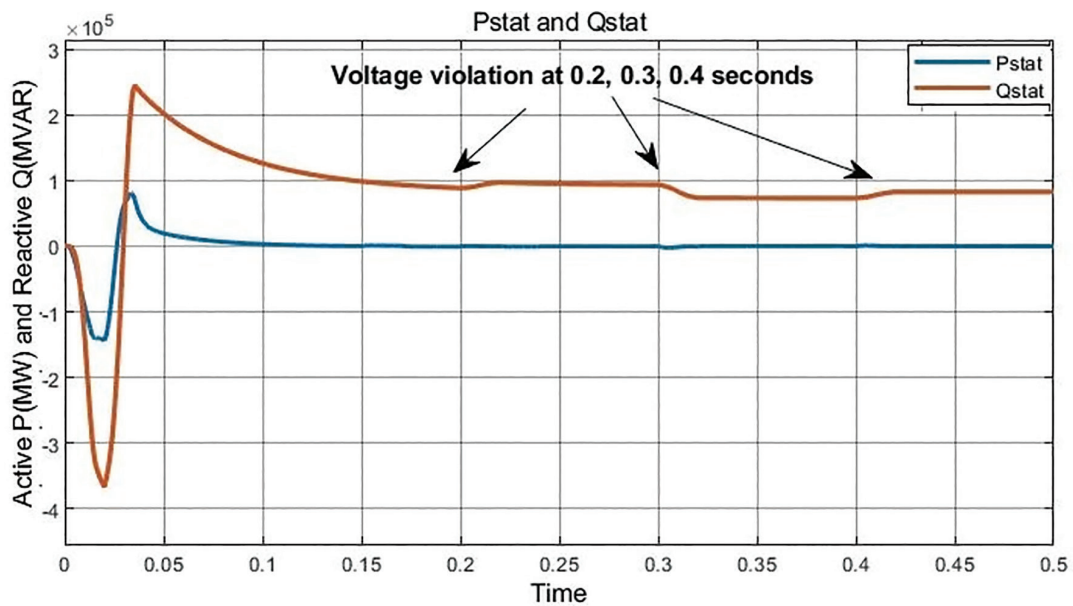**Figure 10.** Source Current (I_r) and Percentage of THD during Non-Linear Load. THD, total harmonic distortion.

Figure 11. $P_{statcom}$ and $Q_{statcom}$ during Voltage Violation at Source End.
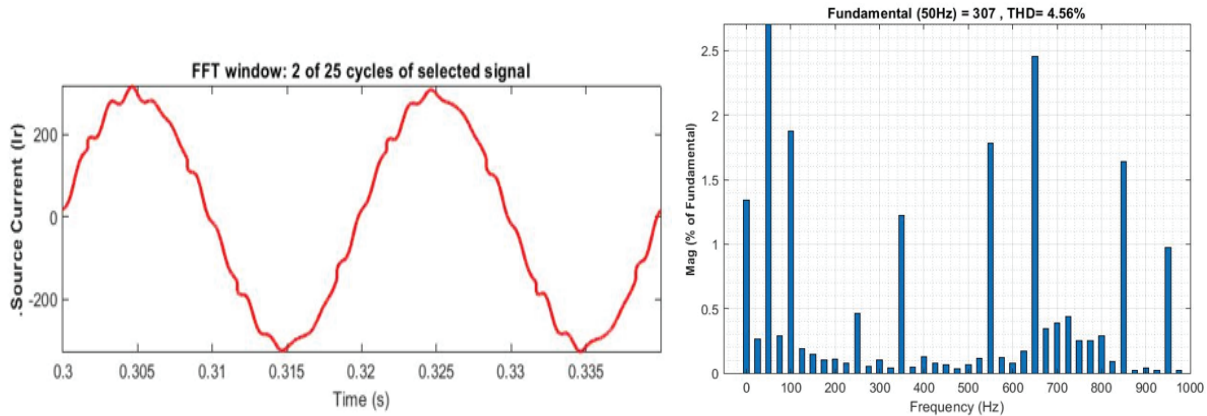
Figure 12. Source Current (I_r) and Percentage of THD during Voltage Violation at Source End. THD, total harmonic distortion.
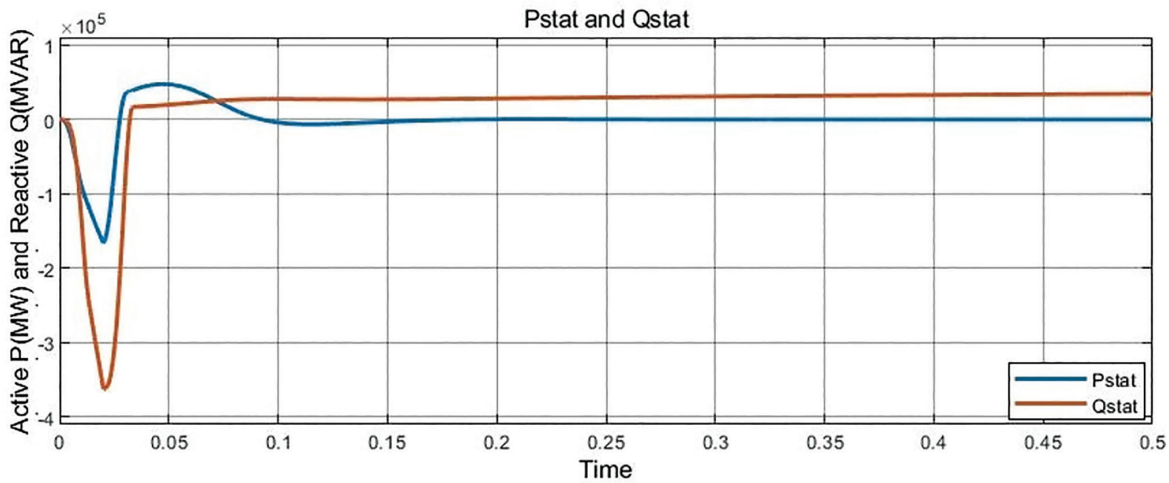

Figure 13. $P_{statcom}$ and $Q_{statcom}$.

5.2. PI with hysteresis current control (HCC)

To ensure the achievability of the proposed methodology to compensate reactive power and suppress percentage THD, the PI with hysteresis current control (HCC) is simulated. The results discuss the above-mentioned cases. Furthermore, the capability of the proposed DSTATCOM to improve power quality is observed through HCC compared to PWM control (Deng, 2007).

Case 1: P_L = 100 kW and Q_L = 75 kVAR

To confirm the probability of the proposed methodology compensating reactive power from the figure 13, the HCC method is applied in this case, where the percentage THD is 0.72 in figure 14. Thus, the proposed system performs very well to improve power quality compared to other methods.

Case 2: Performance Under extra load P = 50 kW, Q = 7.5 kVAR with Load Breaker Closed Unexpectedly

The load breaker is closed at 0.15 s, and in addition to that, the extra load of 50 kW and 7.5 kVAR relates to the network. A trivial variation is observed in the reactive power for a limited time as shown in figure 15. Interestingly, the THD is 0.80 observed in the source current of the R phase from the harmonic spectra in figure 16.

Case 3: Non-Linear Load

In this case, from the figure 17 the performance of the HCC is tested in the presence of a non-linear load. In the presence of the RL load, in addition to that, at 0.15 s, the non-linear load is connected, and not much variation is
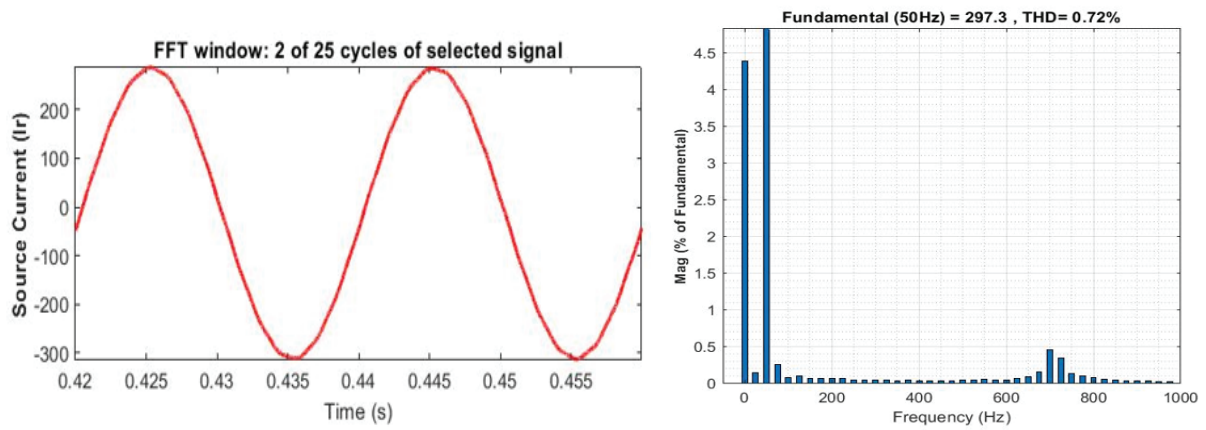
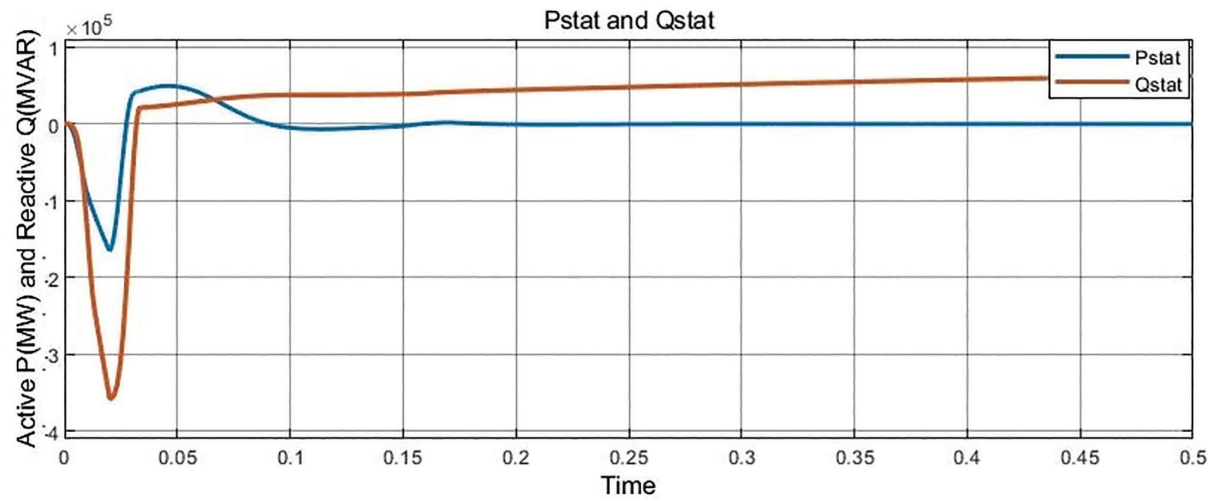**Figure 14.** Source Current (I_r) and Percentage of THD with HCC method. THD, total harmonic distortion.

Figure 15. $P_{statcom}$ and $Q_{statcom}$ Load Breaker Closed Unexpectedly.
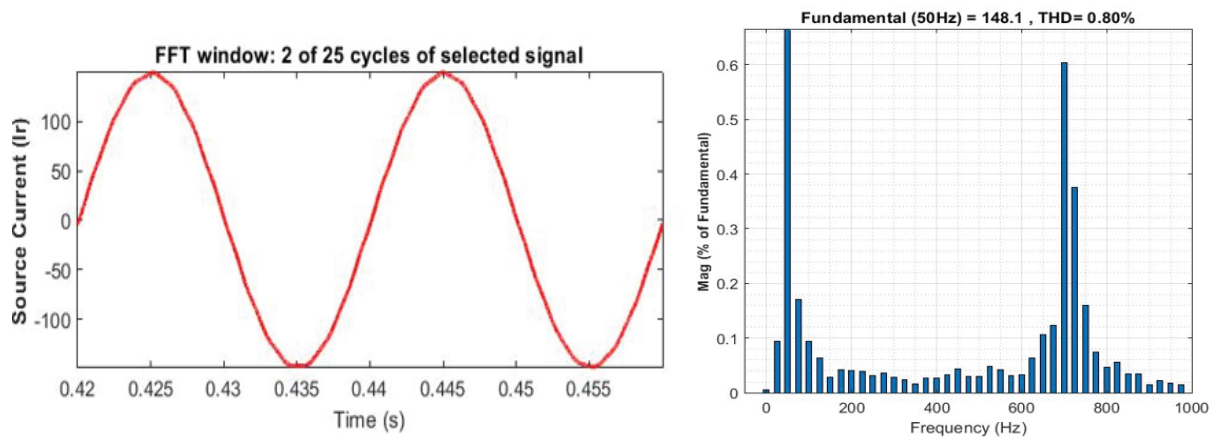
Figure 16. Source Current (I_r) and Percentage of THD during breaker closed with HCC method. THD, total harmonic distortion.
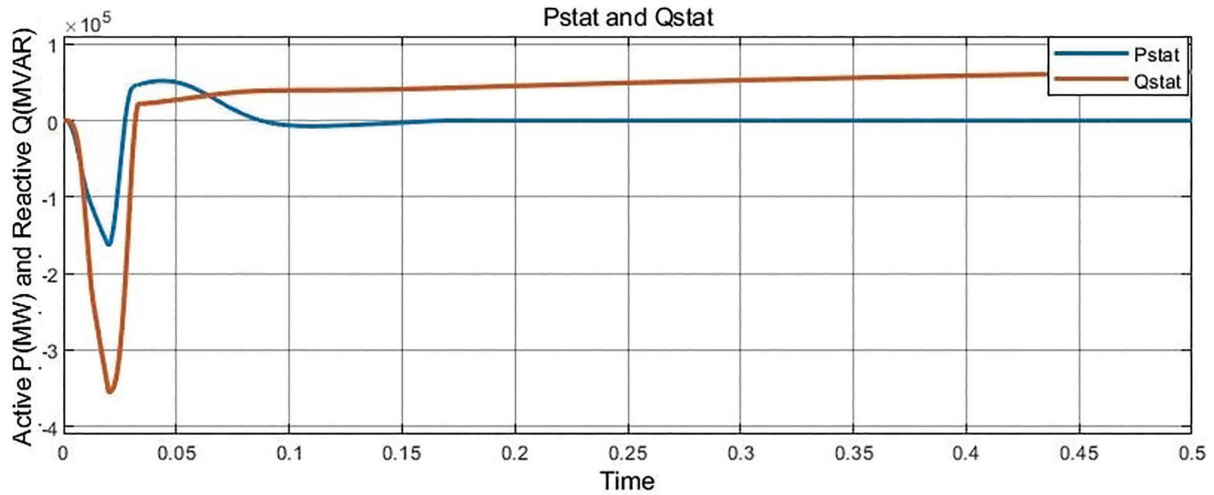
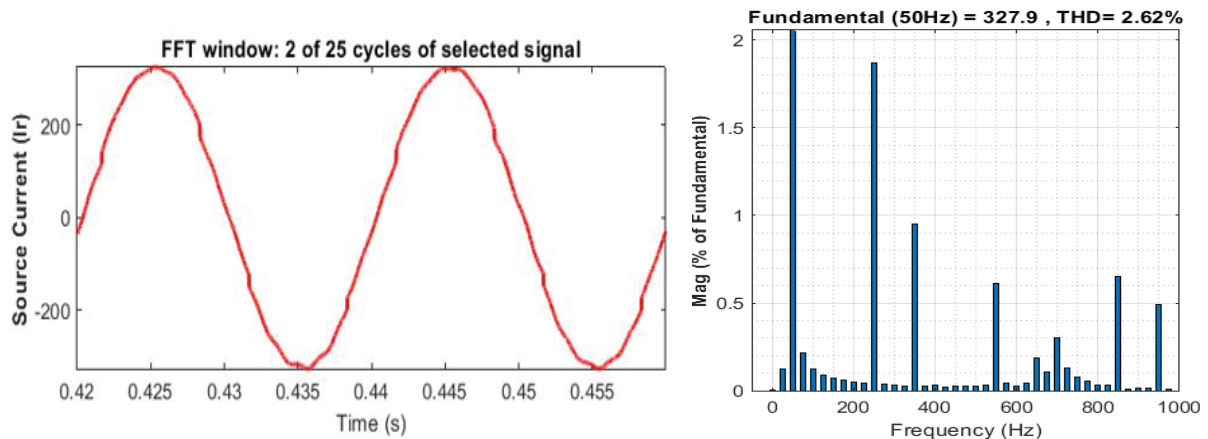**Figure 17.** P$_{statcom}$ and Q$_{statcom}$ Non-Linear Load.

Figure 18. Source Current (I$_r$) and Percentage of THD during Non-linear Load with HCC method. THD, total harmonic distortion.

observed in the active and reactive power. However, the THD is reduced to 2.79 and found to be better than the PWM method from the figure 18 (Raju et al., 2020).

Case 4: Voltage violations at source end with Non-Linear Load

Here, the programmable voltage source is used, and violations in voltage (figure 19) created at different instants are depicted in an enlarge view of waveforms to observe the performance of the proposed DSTSTCOM hysteresis current controller as given in figure 20. The voltage source is programmed at 0.2 s, 0.3 s and 0.4 s by the variation; its value is 6% in the first two cases, and at 0.4 s it is the same as before 0.2 s. The variation in voltage at PCC and reactive power is observed. The enlarged view of the power waveform signifies that at 0.2 s, 0.3 s and 0.4 s, the reactive observed 45 kVAR, 57 kVAR and 55 kVAR, respectively. Though there is a non-linear load, the percentage of THD is 2.65 as presented in figure 21.

The percentage of THD focused in all cases on source current (I$_r$). In the different scenarios observed, however, the percentage of THD in HCC is less than that of the PWM technique. Table 3 (Deng, 2007) represents the THD comparisons of both methods. Nevertheless, HCC proved superior to suppressing harmonic distortion in all different conditions compared to PWM techniques. Table 3 shows the comparisons carried out for THD between PWM, HCC and the current control band HCC. It is possible to notice that the switching frequency changes when the hysteresis control band varies. When the band increases, the current will need more time to reach, and hence the overall
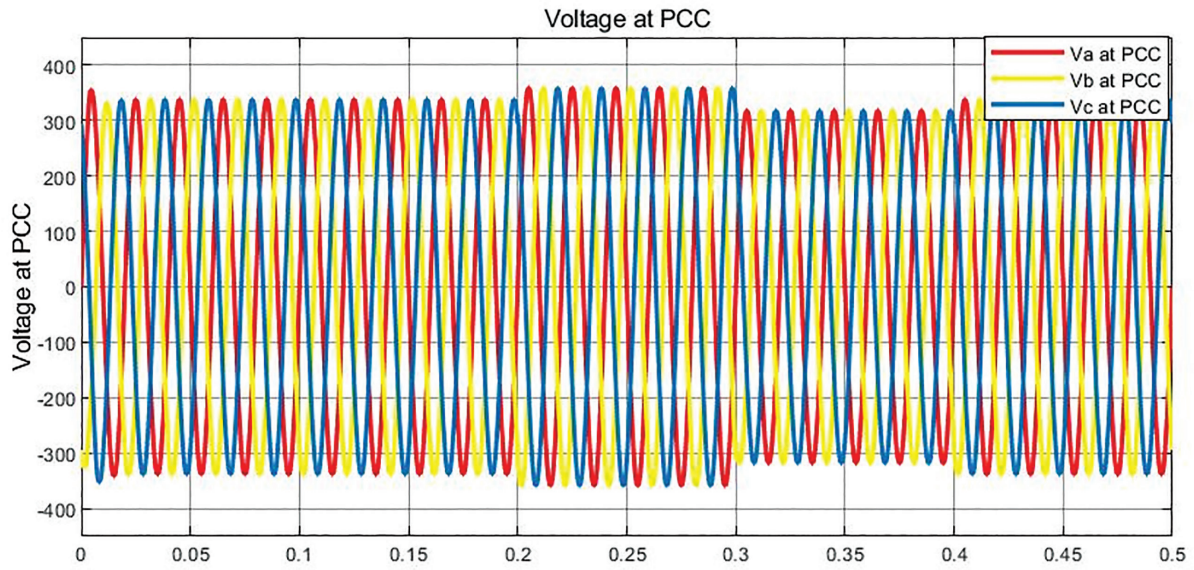
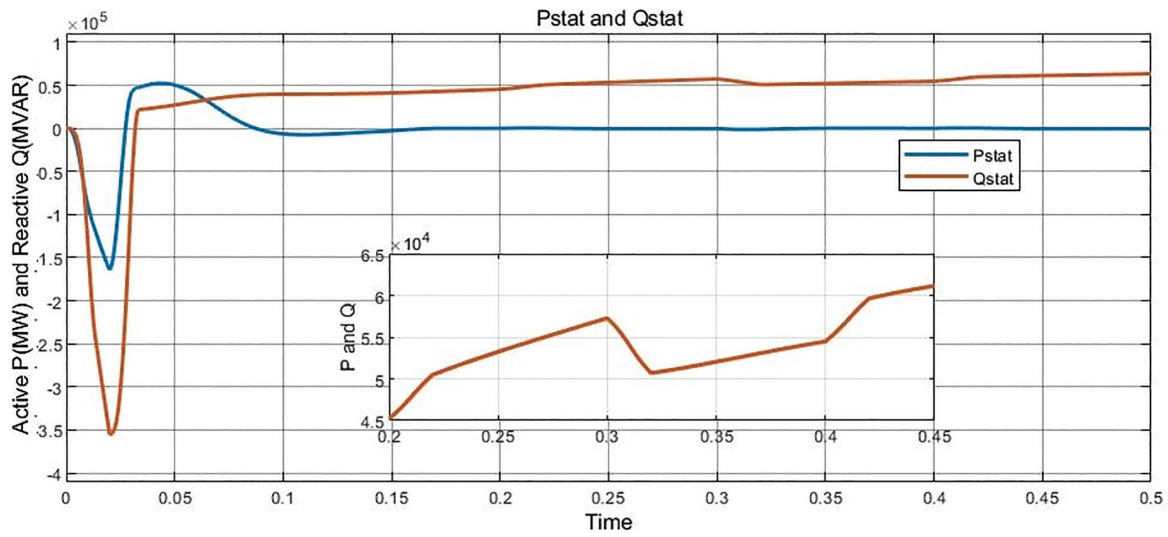**Figure 19.** Voltage at PCC. PCC, point of common coupling.

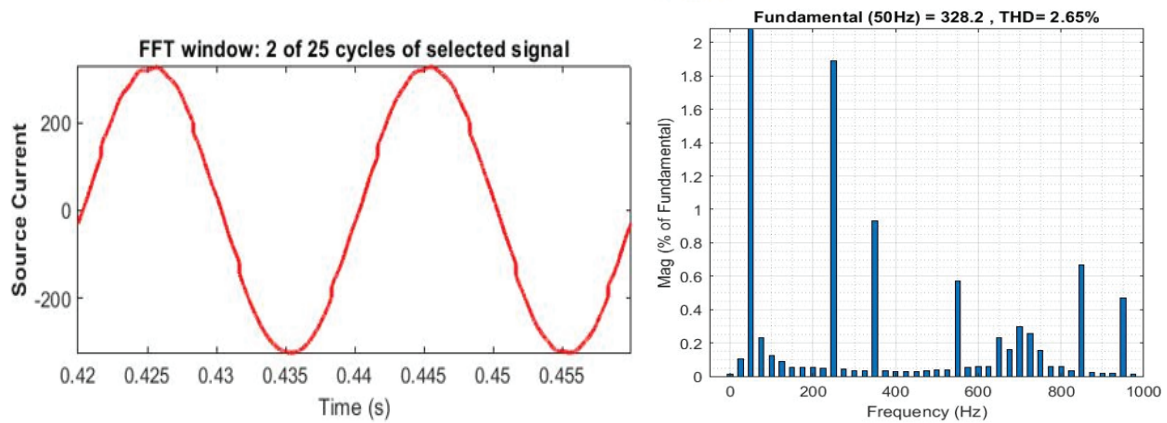**Figure 20.** P~statcom~ and Q~statcom~ Voltage Violation at Source End.

Figure 21. Source Current (I_r) and Percentage of THD during Voltage violation with HCC method. THD, total harmonic distortion.

Table 3. THD analysis with different methods and conditions.

Case	1	2	3	4
PWM (%THD in I_r)	0.82	2.79	4.13	4.56
HCC (%THD in I_r) (Current control band 1%)	0.72	0.80	2.79	2.65
HCC (%THD in I_r) (Current control band 2.5%)	0.87	0.98	3.80	2.65
HCC (%THD in I_r) (Current control band 5%)	0.95	1.20	3.80	2.70

PWM, Pulse Width Modulation; THD, total harmonic distortion.

system performance will change. However, it is observed that by varying the band, there is not much impact on the generation of reactive power from DSTATCOM, but it is noticeable that in the majority of all the cases discussed here, the hysteresis controller is superior to the PWM controller in the reduction of harmonics. However, it is also perceived that by varying the width of the HB, the THD remains under the limit as per the IEEE 519–1992 standard.

6. Conclusions

A detailed dynamic model of DSTATCOM and its control is proposed, developed and implemented in MATLAB, including an effective start-up technique of PWM and hysteresis current control (HCC) with a PI controller in the distribution network. The result analysis shows the effectiveness of the proposed scheme to compensate for the demand for reactive power. It is perceived that the system voltage deviates from its minimum at the time of disturbance. Different cases were discussed and analysed with various conditions to validate the healthier harmonic tracking capability of the proposed DSTATCOM control method. The THD of the compensated source currents in all cases of PWM and HCC control is found to be within the limits of the IEEE-519 standard. However, the harmonic spectra of the HCC technique show greater effectiveness in reducing harmonics than the PWM technique in each case. It is also observed that by increasing the HB, in the majority of cases, THD reduction is superior to the same converter commanded by PWM techniques. Further, experimental analysis will be carried out to study the relationship between switching frequency, voltage drop, actual output current and percentage THD during different loading conditions to deduce a more accurate mathematical model for DSTATCOM control.

References

Amoozegar, D. (2016). DSTATCOM Modelling for Voltage Stability with Fuzzy Logic PI Current Controller. *International Journal of Electrical Power & Energy Systems*, 76, pp. 129–135. doi: 10.1016/j.ijepes.2015.09.017.

Bollen, M. (1999). Understanding Power Quality Problems: Voltage Sags and Interruptions. New York: IEEE Press.

Chebabhi, M. (2016). Four leg D-STATCOM Based on Synchronous Reference Frame Theory with Enhanced Phase Locked Loop for Compensating a Four-Wire Distribution Network under Unbalanced PCC Voltages and loads. *Journal of Power Technology*, Vol.96 (1), pp.15–26.

Chothani, N., Joshi, M., Patel, D. and Raichura, M. (2021). Adaptive PID controller based static var compensation in EHV transmission line. In: *IEEE International Conference on Communication information and Computing Technology (ICCICT)*, June 25–27, IEEE, India,2021.

Daniel, A. and Ramin, M. (2018). Hysteresis band current control applied to a five- level NPC type G converter. In: 13th *IEEE International Conference on Industry Applications*, IEEE, Brazil, pp. 17–23.

Deng, Y. (2007). A Comparison between STATCOMs using PWM Voltage Control and Hysteresis Current Control (HCC). Concordia University, Canada, pp. 1–115.

Edris, A. (2000). FACTS Technology Development: An Update. *Power Engineering Review*, 20(3), pp. 599–627. doi: 10.1109/39.825623.

Eun, S. and Sang, J. (2004). A novel hysteresis current controller to reduce the switching frequency and current error in D-STATCOM. In: *IEEE International Conference Industrial Electronics Society*.

Hingorani, N. G. and Gyugyl, L. (1999). Understanding FACTS: Concepts and Technology of Flexible AC Transmission Systems. Wiley-IEEE Press, USA.

Kalyanraj, D. and Lenin Prakash, S. (2014). Design and Digital Implementation of Constant Frequency Hysteresis Current Controller for Three-Phase Voltage Source Inverter using TMS320F2812. *International Journal of Emerging Electric Power Systems*, 15(1), pp. 13–23. doi: 10.1515/ijeeps-2013-0141.

Kamel, E. and Fenghua, G. (2020). Modelling and Design of the Improved D-STATCOM Control for Power Distribution Grid. *Springer Nature Switzerland*, 2, p. 1519.

Khatir, M., ZidiI, A., Fellah, M., Hadjeri, S. and Flitti, M. (2012). The Impact Study of a STATCOM on Communication Failure in an HVDC Inverter Feeding a weak AC System. *Journal of Electrical Engineering*, 63(2), pp. 95–102.

Li, S., Xu, L. and Haskew, T. (2013). Control of VSC-based STATCOM Using Conventional and Direct-Current Vector Control Strategies. *International Journal of Electrical Power & Energy Systems*, 45(1), pp. 175–186.

Liu, X., Wang, J. and Yao, G. (2012). A Novel Hysteresis Current Control Strategy with Fuzzy Bandwidth for Active Power Filter. *Elektronika ir Elektrotechnika*, 4, pp. 3–8.

Mangaraj, M. and Sabat, J. (2023). Evaluation of SVC-Coupled Hybrid DSTATCOM using JLMS Algorithm for Enhancement of Power Quality. *Power Electronics and Drives*, 8(43), pp. 21–30.

Marei, M. I., El Saadany, E. F. and Salama, M. M. A. (2004). A novel control scheme for STATCOM using space vector modulation-based hysteresis current controller. In: *2004 11th International Conference on Harmonics and Quality of Power (IEEE Cat. No.04EX951)*, 12–15 September 2004, Lake Placid, NY, USA: IEEE. doi: 10.1109/ICHQP.2004.1409329.

Ngasop, N. and David, A. (2020). Using Hysteresis Band Method for the Control of Three-Phase STATCOM Connected to a Transport Network. *European Journal of Engineering Research and Science*, 5(7). doi: 10.24018/ejers.2020.5.7.1983.

Pal, Y., Swarup, A. and Singh, B. (2011). A Control Strategy Based on UTT and Icosϕ Theory of Three-Phase, Four-Wire UPQC for Power Quality Improvement. *International Journal of Engineering Science Technology*, 3(1), pp. 30–40.

Pasrba, J. (2004). How FACTS Controllers Benefit AC Transmission Systems. *Power Engineering Society General Meeting*, 2, pp. 1257–1262.

Rahim, A. H. M. A. and Kandlawala, M. F. (2004). Robust STATCOM Voltage Controller Design Using Loop-Shaping Technique. *Electric Power Systems Research*, 68(1), pp. 61–74. doi: 10.1016/S0378-7796(03)00153-6.

Raju, A., Cheriyan, E. P. and Rijil, R. (2020). Investigations on STATCOM using Current Error Space Phasor Based Modified Hysteresis Current Controller. IETGTD, WILEY, 2020

Safari, A., Ahmadian, A. and Golkar, M. (2013). Comparison of Honey Bee Mating Optimization and Genetic Algorithm for Coordinated Design of PSS and STATCOM based on Damping of Power System Oscillation. *Journal of Electrical Engineering*, 64(3), pp. 133–142.

Singh, B., Dube, S. and Arya, S. (2015). An Improved Control Algorithm of DSTATCOM for Power Quality Improvement. *International Journal of Electrical Power & Energy Systems*, 64, pp. 493–504. doi: 10.1016/j.ijepes.2014.07.055.

Tripathi, S. (2018). Design and Control of a STATCOM for Non-Linear Load Compensation: A Simple Approach. *Riga Technical University*, 14(2), pp. 172–184.